Journal of Sound and Vibration (1999) **220**(1), 117–133
Article No. jsvi.1998.1941, available online at http://www.idealibrary.com on IDEAL

ACOUSTIC RADIATION FROM A RECTANGULAR PLATE REINFORCED BY SPRINGS AT ARBITRARY LOCATIONS

W. L. Li and H. J. Gibeling†

United Technologies Carrier Corporation, Carrier Parkway, Syracuse, NY 13221, *U.S.A.*

(*Received* 11 *June* 1998, *and in final form* 28 *August* 1998)

The vibration of a simply supported rectangular plate which is reinforced by a finite number of springs at arbitrary locations is sought as a linear combination of the flexural modes of the corresponding unloaded (or simple) plate. Although these modes cannot be directly used to decouple the dynamic equations of the motion of the reinforced plate, it is still advantageous to use them as a complete set of basis functions to represent the interested quantities such as the deflection of the plate. A linear transformation is established between the two modal spaces spanned by the modes, respectively, for the reinforced and the unloaded plates. The radiation characteristics of the spring-reinforced plate are investigated by using a near field formulation. In order to reduce computational burden, a frequency interpolation technique is employed so that numerical integration now needs to be carried out only at some key frequencies. The specific radiation resistances of the basis modes are first determined as a set of invariants from which the modal radiation efficiency of the reinforced plate can be readily extracted. The effects of cross-modal coupling between the basis modes have been considered, which is necessary for an accurate determination of the modal radiation efficiency for the reinforced plate. A qualitative procedure is also described for locating the "coincidence" frequencies where the modal radiation efficiencies of the reinforced plate tend to reach their peak values.

1. INTRODUCTION

Many structures of practical concerns may be adequately approximated by a rectangular plate. Their vibro–acoustic characteristics may well be understood or inferred from studying the much simpler plate problems. As a result, the vibration of and acoustic radiation from plates with various complications have long been an important subject in structural dynamics and acoustics. The problem of a rectangular plate having a rigid mass of finite width running across its center was studied by Cohen and Handelman [1]. The Rayleigh–Ritz method was used by assuming a simple polynomial form of mode shape. The vibrations of plates carrying a concentrated mass was investigated in references [2, 3] where the flexural

† Current address: Applied Research Laboratory, Pennsylvania State University, State College, PA16801, U.S.A.

0022–460X/99/060117 + 17 $30.00/0

displacement was expanded as a double series of mode shapes for the unloaded plate. The characteristic equation for the natural frequencies of the plate–mass system was derived by enforcing the compatibility conditions at the mass location(s). A general variational formulation was given by Stokey and Zorowski [4] for the determination of the natural frequencies of a plate carrying a finite number of masses. However, it was shown that the accuracy of natural frequencies so estimated was quite sensitive to the locations of the masses. Recently, the vibration of plates loaded with any number of masses or springs was solved in references [5, 6] by using a so-called Analytical-and-Numerical-Combined Method (ANCM). Unlike many analytical methods being practical only for plates with a single concentrated element (spring or mass), ANCM allows a simple and unified solution for plates carrying any number of elements. A systematic discussion about plate vibrations can be found in reference [7].

The radiation of sounds from rectangular plates was investigated by many authors. Wallace [8] presented an asymptotic solution for the radiation efficiencies of different plate modes at low frequencies. It was shown that the total power radiated from the whole plate is actually bounded by that from a single intranodal area when the acoustic wavelength greatly exceeds the structural wavelengths in both directions. The sound radiation under general boundary conditions was considered by Gomperts [9] and Berry *et al*. [10]. In the literature, the radiation characteristics were mostly studied based on the farfield sounds, which often admit a closed-form of solutions for large or small acoustic wavenumber. In a medium frequency range, the radiated power can be expressed as a double integral that is generally calculated numerically. The plate radiation problems were also investigated in references [11, 12] by using a near field formulation in which the modal radiation efficiency is originally represented by a quadruple integral. A co-ordinate transformation technique was utilized to convert the quadruple integral into a sum of single integrals. In most investigations, the radiated sound power is simply determined from the modal radiation efficiencies, without considering the cross-modal contributions. Keltie and Peng [13] studied the effects of cross-modal coupling on the sound radiation from plates of infinite long and finite width. It was shown that the contributions due to cross-modal coupling may be important at low frequency or if the plate is under an off-resonant excitation. Snyder and Tanaka demonstrated that the coupling terms could be simply obtained from the modal radiation efficiencies [14]. Their formulae, however, are valid only for small wavenumbers. Li and Gibeling [15] studied, in a general manner, the characteristics of the cross-modal coupling and its impacts on the power radiation. It was shown that the mutual terms (radiation resistances) resulting from the cross-modal coupling can be determined easily and accurately in the whole frequency range.

In this paper, the vibration of a simply supported rectangular plate which is reinforced by a finite number of springs at arbitrary locations is sought as a linear combination of the flexural modes of the corresponding unloaded (or simple) plate. Although these modes cannot be directly used to decouple the dynamic equations of the motion of the reinforced plate, it is still advantageous to use them as a complete set of basis functions to represent the interested quantities such as

the deflection of the plate. A linear transformation is established between the two modal spaces spanned by the modes, respectively, for the reinforced and the unloaded plates. The radiation characteristics of the spring-reinforced plate are investigated by using a near field formulation. In order to reduce computational burden, a frequency interpolation technique is employed so that numerical integration now needs to be carried out only at some key frequencies. The specific radiation resistances of the basis modes are first determined as a set of invariants from which the modal radiation efficiency of the reinforced plate can be readily extracted. The effects of cross-modal coupling between the basis modes have been considered, which is necessary for an accurate determination of the modal radiation efficiency for the reinforced plate. A qualitative procedure is also described for locating the "coincidence" frequencies where the modal radiation efficiencies of the reinforced plate tend to reach their peak values.

2. VIBRATION OF A SPRINGS-REINFORCED PLATE

Consider a thin rectangular plate of length a and width b reinforced through N_k springs at arbitrary points, as shown in Figure 1. The differential equation for the flexural displacement, w, of the plate is given by

$$\left\{ D\nabla^4 + \mathrm{i}c\omega - \rho h\omega^2 + \sum_{i=1}^{N_k} k_i \delta(x - x_i, y - y_i) \right\} w = P(x, y), \tag{1}$$

where $D = Eh^3/12(1 - v^2)$ is the bending stiffness of the plate, ω is the angular frequency, E is the Young's modulus, v is the Poisson's ratio, c is the damping coefficient of the plate material, ρ is the plate mass per unit area, h is plate thickness, $P(x, y)$ is the pressure, δ is the Dirac delta function, and k_i is the spring constant at location (x_i, y_i).

Various techniques have been exploited to solve equation (1). Here, however, the one used in references [5, 6] will be presented because of its simplicity and generality.

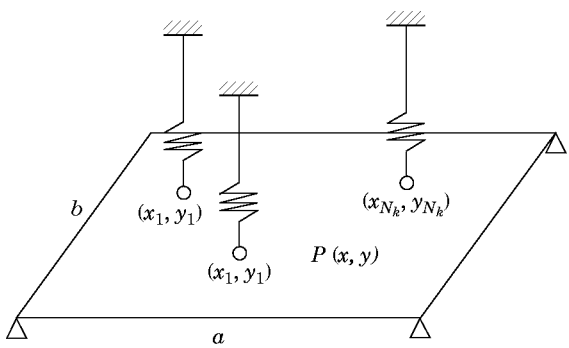

Figure 1. Schematic of a rectangular plate reinforced by finite springs.

In the absence of the springs, the solution of equation (1) is typically expressed as a double series of the flexural modes:

$$w = \sum_{m=1}^{\infty} \sum_{n=1}^{\infty} A_{mn} \psi_{mn}(x, y), \tag{2}$$

or

$$w = \boldsymbol{\Psi}^{\mathrm{T}} \mathbf{A}, \tag{3}$$

where A_{mn} is the expansion coefficient, and ψ_{mn} is the (m, n) bending mode of the plate. For a simply-supported plate, it is well known that

$$\psi_{mn}(x, y) = (2/\sqrt{ab}) \sin (m\pi/a)x \sin (n\pi/a)y. \tag{4}$$

Substituting equation (4) into equation (1) and making use of the orthogonality of the modes, one has

$$A_{mn} = \frac{\langle \psi_{mn}, P \rangle}{[\rho h(\omega_{mn}^2 - \omega^2) + \mathrm{i}\omega c]}, \tag{5}$$

where $\langle u, v \rangle = \int_0^b \int_0^a u(x, y) v(x, y)\, \mathrm{d}x\, \mathrm{d}y$ and $\omega_{mn} = \sqrt{D/\rho h}[(m\pi/a)^2 + (n\pi/b)^2]$ is the natural frequency of the (m, n) mode.

Equation (5) indicates that in the modal space the expansion coefficients can be independently determined with no need for solving a set of linear algebraic equations. However, when springs are attached to the plate, the modes (or basis modes when a distinction needs to be made from the current modes for the reinforced plate) given by equation (4) will all be modified, except for those whose nodal lines contain all the attachment points. Hence, they are normally not the modes of the reinforced plate. However, equation (2) is still usable in view of the completeness of the characteristic functions (or modes), and the unknown expansion coefficients will now have to be determined from

$$(\boldsymbol{\Omega} + \mathrm{i}\omega c\mathbf{I} - \rho h\omega^2 \mathrm{I} + \mathbf{K})\mathbf{A} = \mathbf{P}, \tag{7}$$

where

$$\Omega_{mn,m'n'} = \rho h \omega_{mn}^2 \delta_{mm'} \delta_{nn'}, \tag{8}$$

$$K_{mn,m'n'} = \sum_i k_i \psi_{mn}(x_i, y_i) \psi_{m'n'}(x_i, y_i), \qquad P_{mn} = \langle \psi_{mn}, P \rangle, \tag{9, 10}$$

$\mathbf{I}$ is the identity matrix and δ_{mn} is the Kronecker delta.

It is clear from equation (7) that one now needs to solve a set of linear equations to determine the expansion coefficients, hence the vibration of the plate. Because of the explicit inclusion of frequency in the coefficient matrix, the expansion coefficients are obviously frequency dependent and have to be solved at each frequency step, which is obviously not efficient when a solution is desired at a large

number of frequencies. In order to avoid this difficulty, consider a linear space $\underline{\Phi}$ of MN dimension spanned by the vectors $\boldsymbol{\phi}_i$ satisfying

$$(\boldsymbol{\Omega} + \mathbf{K})\boldsymbol{\phi}_i - \lambda_i \boldsymbol{\phi}_i = 0, \qquad i = 1, 2, \cdots, MN; \quad \text{and} \quad \boldsymbol{\phi}_i^{\mathrm{T}} \boldsymbol{\phi}_j = \delta_{ij}. \quad (11, 12)$$

Such a space is complete, a useful property of eigenvectors. Thus, the coefficient vector $\mathbf{A}$ can be expressed as

$$\mathbf{A} = \boldsymbol{\Phi}\boldsymbol{\alpha}, \tag{13}$$

where

$$\boldsymbol{\Phi} = [\boldsymbol{\phi}_1, \boldsymbol{\phi}_2, \cdots, \boldsymbol{\phi}_{mn}, \cdots, \boldsymbol{\phi}_{MN}]. \tag{14}$$

Substituting equation (13) into equation (7) and left-multiplying it with $\boldsymbol{\Phi}^{\mathrm{T}}$ leads to

$$\boldsymbol{\alpha} = [\boldsymbol{\Lambda} + \mathrm{i}\omega c\mathbf{I} - \rho h\omega^2 \mathbf{I}]^{-1} \boldsymbol{\Phi}^{\mathrm{T}} \mathbf{P}, \tag{15}$$

where

$$\boldsymbol{\Lambda} = \mathrm{diag}[\lambda_1, \lambda_2, \cdots, \lambda_{MN}]. \tag{16}$$

Inserting equations (13) and (15) into equation (3), the vibration of the plate can be finally obtained as

$$w = \sum_j \frac{\boldsymbol{\Psi}^{\mathrm{T}} \boldsymbol{\phi}_j \boldsymbol{\phi}_j^{\mathrm{T}} \langle \boldsymbol{\Psi}, P \rangle}{\lambda_j + \mathrm{i}\omega c - \rho h \omega^2}. \tag{17}$$

In the above discussion, the truncated form of equation (2) has been assumed with $m = 1, 2, \cdots, M$ and $n = 1, 2, \cdots, N (MN = M \times N)$.

It is easy to verify that the vector $\boldsymbol{\Psi}^{\mathrm{T}} \boldsymbol{\phi}_i$ is simply the ith mode of the spring-reinforced plate whose natural frequency is given by $\omega_i = \sqrt{\lambda_i / \rho h}$. Define $\underline{\Psi}$ as the linear space spanned by ψ_{mn}'s, $m = 1, 2, \cdots, M$ and $n = 1, 2, \cdots, N$. Then the (m,n)th component of the vector $\boldsymbol{\phi}_i$ simply specifies the co-ordinate of the mode $\boldsymbol{\Psi}^{\mathrm{T}} \boldsymbol{\phi}_i$ in the ψ_{mn}-axis. In other words, the matrix $\boldsymbol{\Phi}$ defines a linear mapping or relationship between the basis modes and the current modes for the reinforced plate.

3. SOUND RADIATION FROM THE PLATE

The sound field generated by an infinitely-baffled rectangular plate can be obtained from the well-known Raleigh integral:

$$p(x, y, z) = \frac{\mathrm{i}\omega\rho_0}{2\pi} \int_0^b \int_0^a \frac{\dot{w}\, \mathrm{e}^{-\mathrm{i}k\sqrt{(x-x')^2 + (y-y')^2 + z^2}}}{\sqrt{(x-x')^2 + (y-y')^2 + z^2}} \, \mathrm{d}x' \, \mathrm{d}y', \tag{18}$$

where ρ_0 is the density of air and k is the acoustic wavenumber.

The total sound power is calculated by integrating the sound intensity over the whole plate area:

$$W = \langle \tfrac{1}{2} \Re[\dot{w}^*, p|_{z=0}] \rangle, \tag{19}$$

where * and $\Re$ denote the complex conjugate and the real part of a complex number, respectively. Substitution of equations (2), (13) and (18) into equation (19) yields

$$W = \tfrac{1}{2}\rho_0 c_0 \omega^2 (\boldsymbol{\alpha}^{\mathrm{H}} \boldsymbol{\Phi}^{\mathrm{T}} \Re[\mathbf{Z}] \boldsymbol{\Phi} \boldsymbol{\alpha}), \tag{20}$$

where c_0 is the wave speed in air, the superscript H denotes the Hermitian operation and $Z_{mn,n'm'} = \zeta_{mn,n'm'} + \mathrm{i}\chi_{mn,n'm'}$ is the specific radiation impedance (ratio), defined as

$$\zeta_{mn,n'm'} = \frac{k}{2\pi} \int_0^b \int_0^a \int_0^b \int_0^a \psi_{mn}(x, y) \psi_{m'n'}(x', y') \times \frac{\sin k\sqrt{(x - x')^2 + (y - y')^2}}{\sqrt{(x - x')^2 + (y - y')^2}} \, \mathrm{d}x' \, \mathrm{d}y' \, \mathrm{d}x \, \mathrm{d}y, \tag{21}$$

$$\chi_{mn,m'n'} = \frac{k}{2\pi} \int_0^b \int_0^a \int_0^b \int_0^a \psi_{mn}(x, y) \psi_{m'n'}(x', y') \times \frac{\cos k\sqrt{(x - x')^2 + (y - y')^2}}{\sqrt{(x - x')^2 + (y - y')^2}} \, \mathrm{d}x' \, \mathrm{d}y' \, \mathrm{d}x \, \mathrm{d}y. \tag{22}$$

Accordingly, the radiation efficiency for the ith mode of the spring-reinforced plate can be calculated from

$$\sigma_i = \boldsymbol{\phi}_{\mathrm{i}}^{\mathrm{T}} \Re[\mathbf{Z}] \boldsymbol{\phi}_i. \tag{23}$$

The radiated sound power is usually determined by including only the self-radiation resistances, the diagonal elements ($m = m'$ and $n = n'$) in $\Re[\mathbf{Z}]$, which may be adequate when a plate vibrates under a resonant condition and the dominant modes are well separated. As a result, one can avoid the calculation of the mutual radiation resistances represented by the off-diagonal elements. It is obvious, however, from equation (23) that the mutual radiation resistances will need to be taken into account in determining the modal radiation efficiency for the reinforced plate because the contributions of the self and mutual terms are now completely tangled up through the eigenvector $\boldsymbol{\phi}_i$. The arbitrariness of a reinforcing plan, hence of the eigenvector $\boldsymbol{\phi}_i$, prohibits one from making any general assumption that the effects of the mutual terms can be safely ignored.

The determination of the radiation resistance matrix $\Re[\mathbf{Z}]$ involves calculating the quadruple integral given in equation (21), which is a computing intensive task, especially at high frequencies because of the rapid oscillation of the integrands. In order to alleviate this problem, the quadruple integral is typically converted into several double integrals via a co-ordinate transformation [11, 12]. The self radiation resistances can then be expressed as

$$\zeta_{mn,mn} = (1/\alpha_m \beta_n) J_1^{mn} + J_2^{mn} + (1/\alpha_m) J_3^{mn} + (1/\beta_n) J_4^{mn}, \tag{24}$$

where

$$\begin{Bmatrix} J_1^{mn} \\ J_2^{mn} \\ J_3^{mn} \\ J_4^{mn} \end{Bmatrix} = \frac{2k}{\pi ab} \int_0^b \int_0^a \begin{Bmatrix} 1 \\ (a-\kappa)(b-\tau) \\ (b-\tau) \\ (a-\kappa) \end{Bmatrix} \begin{Bmatrix} \sin \alpha_m \kappa \sin \beta_n \tau \\ \cos \alpha_m \kappa \cos \beta_n \tau \\ \sin \alpha_m \kappa \cos \beta_n \tau \\ \cos \alpha_m \kappa \sin \beta_n \tau \end{Bmatrix}$$

$$\times \frac{\sin k\sqrt{\kappa^2 + \tau^2}}{\sqrt{\kappa^2 + \tau^2}} \, \mathrm{d}\kappa \, \mathrm{d}\tau. \tag{25}$$

Similarly, the mutual radiation resistance can be written as [15]:
for $m' \neq m$ and $n' \neq n$,

$$\zeta_{mn,m'n'} = \frac{\epsilon(m'-m)\epsilon(n'-n)}{(\alpha_m^2 - \alpha_{m'}^2)(\beta_n^2 - \beta_{n'}^2)} \{\alpha_m \beta_n J_1^{m'n'} - \alpha_m \beta_{n'} J_1^{m'n} - \alpha_{m'} \beta_n J_1^{mn'} + \alpha_{m'} \beta_{n'} J_1^{mn}\}; \tag{26}$$

for $m' \neq m$ and $n' = n$,

$$\zeta_{mn,m'n} = [\epsilon(m'-m)/(\alpha_m^2 - \alpha_{m'}^2)]\{\alpha_m J_3^{m'n} - \alpha_{m'} J_3^{mn} + (\alpha_m/\beta_n) J_1^{m'n} - (\alpha_{m'}/\beta_n) J_1^{mn}\}; \tag{27}$$

for $m' = m$ and $n' \neq n$,

$$\zeta_{mn,mn'} = [\epsilon(n'-n)/(\beta_n^2 - \beta_{n'}^2)]\{\beta_n J_4^{mn'} - \beta_{n'} J_4^{mn} + (\beta_n/\alpha_m) J_1^{mn'} - (\beta_{n'}/\alpha_m) J_1^{mn}\}, \tag{28}$$

where

$$\epsilon(m'-m) = \begin{cases} 0, & \text{for} \quad m'-m = \pm 1, \quad \pm 3, \quad \pm 5, \quad \cdots, \\ 2, & \text{for} \quad m'-m = \pm 2, \quad \pm 4, \quad \pm 6, \quad \cdots. \end{cases} \tag{29}$$

The matrix $\Re[\mathbf{Z}]$ is symmetric, which is clear from its original definition, equation (21). In addition, equations (26–28) indicate that it is sparsely populated: about three quarters of its $MN \times MN$ elements are constantly zero. Therefore, there is a total of about $MN^*(MN-1)/8$ off-diagonal elements (or mutual radiation resistances) to be determined, which may still be a devastating problem when a large number of modes are involved. Fortunately, it turns out that all the mutual radiation resistances can be determined at virtually no cost. This is evident from the fact that, since m and m' (also n and n') only take the numbers from the same collection (of integers), all the integrals appearing in equations (26–28) have already been encountered and calculated once in the process of determining the self-radiation resistances.

The double integrals given in equation (25) can be further reduced to several single integrals by performing the integration in a polar co-ordinate system. Such an approach, however, will not be adopted here due to the lengthy expressions

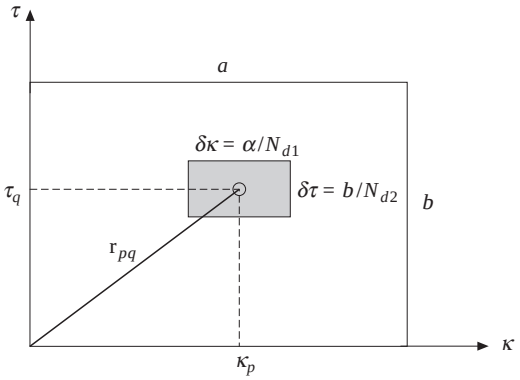

Figure 2. Discretization of the plate.

involved. Instead, a different technique to facilitate the calculations will be employed.

The explicit inclusion of the acoustic wavenumber in the integrands implies that the self and mutual radiation resistances are frequency dependent, and the computing intensive numerical integrations need to be carried out at each frequency. The rapid oscillation of the integrands in the integration domain tends to cause a convergence problem for a large acoustic wavenumber. However, when viewing from a different angle in the wavenumber space, the integrands will show a much simpler (sinusoidal) pattern. This suggests that the frequency interpolation technique discussed in reference [16] may be applicable here. Essentially, it is based on the premise that a function varies so slowly in a frequency range that its values at any (slave) frequency k can be adequately obtained from those at the two end (master) frequencies, k_1 and k_2 that is,

$$\zeta(k) = (1 - \sigma)\zeta(k_1) + \sigma\zeta(k_2), \qquad 0 \leqslant \sigma = (k - k_1)/(k_2 - k_1) \leqslant 1. \tag{30}$$

In equation (30), the function ζ may represent any of the integrals defined in equation (25). In this way, the intensive numerical integrations can now be avoided at slave frequencies.

Examining the frequency dependent terms in equation (25) reveals that all the integrands vary sinusoidally with frequency at any given point (κ, τ), becoming most violent when $\sqrt{\kappa^2 + \tau^2}$ reaches its maximum value $R_m = \sqrt{a^2 + b^2}$. Therefore, how well does the frequency interpolation scheme work for the function $\sin(kR_m)$ will ultimately determine the accuracy of the radiation resistance calculated at the slave frequencies. Apparently, the characteristic size, R_m, of a plate measures the oscillatory frequency of the function $\sin(kR_m)$ in the wavenumber space. For example, it varies slower for a smaller plate. Bearing this in mind, the whole area of a plate will be divided into $N_{d1} \times N_{d2}$ small rectangular ones, as shown in Figure 2.

Accordingly, an integral over $[(0, a)\otimes(0, b)]$ can be expressed as a sum of the integrals over these smaller areas, $S_{pq} = (\kappa_p - \delta\kappa/2,\kappa_p + \delta\kappa/2)\otimes(\tau_q - \delta\tau/2,\tau_q + \delta\tau/2)$, that is,

$$\int_0^b \int_0^a (\cdot) = \sum_{p,q}^{N_{d1},N_{d2}} \int_{\tau_q - \delta\tau/2}^{\tau_q + \delta\tau/2} \int_{\kappa_p - \delta\kappa/2}^{\kappa_p + \delta\kappa/2} (\cdot) = \sum_{p,q} \int_{S_{pq}} (\cdot). \tag{31}$$

Although such a discretization procedure may not add any value to the numerical integrations, it will play a key role in making the interpolation scheme successful. Consider the function

$$\sin k\sqrt{\kappa^2 + \tau^2} = \mathrm{Im}\{\mathrm{e}^{\mathrm{i}k\sqrt{\kappa^2 + \tau^2}}\}. \tag{32}$$

Apply a neutralization factor $\mathrm{e}^{\mathrm{i}kr_{pq}}$ to it:

$$\mathrm{Im}\{\mathrm{e}^{\mathrm{i}k\sqrt{\kappa^2 + \tau^2}}\} = \mathrm{Im}\{\mathrm{e}^{\mathrm{i}k(\sqrt{\kappa^2 + \tau^2} - r_{pq})}\, \mathrm{e}^{\mathrm{i}kr_{pq}}\}. \tag{33}$$

In light of equations (31) and (33), equation (24), for example, can be rewritten as

$$\zeta_{mn,mn} = \sum_{p,q} \mathrm{Im}\left\{\mathrm{e}^{\mathrm{i}kr_{pq}} \int_{S_{pq}} \left[\frac{1}{\alpha_m\beta_n} I_1^{mn} + (a - \kappa)(b - \tau) I_2^{mn} + \frac{(b - \tau)}{\alpha_m} I_3^{mn} + \frac{(a - \kappa)}{\beta_n} I_4^{mn}\right] \mathrm{d}\kappa\, \mathrm{d}\tau\right\} = \sum_{p,q} \mathrm{Im}\{\mathrm{e}^{\mathrm{i}kr_{pq}} \Gamma_{pq}(k)\}, \tag{34}$$

where I_i^{mn} is obtained from J_i^{mn} by simply replacing the term $\sin k\sqrt{\kappa^2 + \tau^2}$ with $\mathrm{e}^{\mathrm{i}k(\sqrt{\kappa^2 + \tau^2} - r_{pq})}$. Now, our problem has been reformulated as: (1) to faithfully calculate $\Gamma_{pq}(k)$ at the master frequencies and (2) to approximate it, at all other frequencies, by using the interpolation technique.

Obviously, the spacing between two master frequencies cannot be arbitrarily large. A criterion on the maximum spacing can be established by considering

$$\begin{aligned}
\Gamma_{pq}(k) &= \int_{S_{pq}} \mathrm{e}^{\mathrm{i}k(\sqrt{\kappa^2 + \tau^2} - r_{pq})} F(\kappa, \tau)\, \mathrm{d}\kappa\, \mathrm{d}\tau \\
&= \int_{S_{pq}} \{1 + \mathrm{i}k(\sqrt{\kappa^2 + \tau^2} - r_{pq}) + \frac{1}{2!}[\mathrm{i}k(\sqrt{\kappa^2 + \tau^2} - r_{pq})]^2 \\
&\quad + \frac{1}{3!}[\mathrm{i}k(\sqrt{\kappa^2 + \tau^2} - r_{pq})]^3 + \cdots\} F(\kappa, \tau)\, \mathrm{d}\kappa\, \mathrm{d}\tau \\
&= \int_{S_{pq}} \{[1 - \frac{k^2}{2!}(\sqrt{\kappa^2 + \tau^2} - r_{pq})^2 + \cdots] + \mathrm{i}k(\sqrt{\kappa^2 + \tau^2} - r_{pq})
\end{aligned}$$

$$\times [1 - \frac{k^2}{3!}(\sqrt{\kappa^2 + \tau^2} - r_{pq})^2 + \cdots]\}F(\kappa, \tau)\,\mathrm{d}\kappa\,\mathrm{d}\tau$$

$$= \int_{S_{pq}} \{1 + \mathrm{i}k(\sqrt{\kappa^2 + \tau^2} - r_{pq}) + \mathcal{O}[k^2(\sqrt{\kappa^2 + \tau^2} - r_{pq})^2]\}F(\kappa, \tau)\,\mathrm{d}\kappa\,\mathrm{d}\tau. \tag{35}$$

Now, it becomes clear that equation (30) is equivalent to accounting for only the first two terms in equation (35). However, its accuracy can be ensured if the following conditions is met:

$$k(\sqrt{\kappa^2 + \tau^2} - r_{pq})^2 \ll 1, \tag{36}$$

$$\forall(\kappa, \tau) \in [(\kappa_p - \delta\kappa/2,\ \kappa_p + \delta\kappa/2) \otimes (\tau_q - \delta\tau/2,\ \tau_q + \delta\tau/2)].$$

Referring to Figure 2, one will have

$$k(\sqrt{\kappa^2 + \tau^2} - r_{pq}) \leqslant \tfrac{1}{2}k\sqrt{\delta\kappa^2 + \delta\tau^2} = \tfrac{1}{2}k\sqrt{(a/N_{d1})^2 + (b/N_{d2})^2}, \tag{37}$$

$$\forall(\kappa, \tau) \in [(\kappa_p - \delta\kappa/2,\ \kappa_p + \delta\kappa/2) \otimes (\tau_q - \delta\tau/2,\ \tau_q + \delta\tau/2)].$$

The number of divisions can be independently selected along each of the plate lengths. However, a better division plan should be such that the final small areas are square-like, i.e., $a/N_{d1} \cong b/N_{d2}$. Under this situation, the condition for the maximum frequency spacing, equation (36), can be explicitly expressed as:

$$k_{\max}\sqrt{2}\,N_{d1}\epsilon/a, \qquad \text{or} \qquad f_{\max} = (c_0\epsilon/\sqrt{2}\,\pi a)N_{d1}, \tag{38, 39}$$

where ϵ is introduced as a small number that sets up the error tolerance.

Equation (39) indicates that the above discretization and neutralization procedure will allow the spacing between two master frequencies to increase by up to a factor of $2N_{d1}$. It needs to be noted that such a discretization process should not compromise the accuracy of numerical integrations, nor will it consume more computing time.

It is clear from equation (35) that for $k(\sqrt{\kappa^2 + \tau^2} - r_{pq}) \leqslant \epsilon < 1$ both the real and imaginary parts of $\Gamma_{pq}(k)$ are a descending series with different signs for any two adjacent terms. Therefore, ϵ^2 will bound the truncation error resulting from dropping all of the higher order terms in the frequency interpolation approximation. For example, for $\epsilon = 0{\cdot}1$, the interpolation error for $\Gamma_{pq}(k)$ will not exceed 1% at any slave frequency. Correspondingly, the resultant radiation resistances are expected to have the same accuracy, if not higher.

4. RESULTS AND DISCUSSIONS

As an example problem, consider a steel plate: $a = 0{\cdot}71$ m, $b = 0{\cdot}74$ m and $h = 0{\cdot}005$ m. Four identical springs ($k_1 = k_2 = k_3 = k_4 = 2{\cdot}4 \times 10^6$ N/m) are attached to the plate at arbitrarily selected locations: $(0{\cdot}3a, 0{\cdot}3b)$, $(0{\cdot}3a, 0{\cdot}6b)$, $(0{\cdot}6a, 0{\cdot}3b)$ and $(0{\cdot}6a, 0{\cdot}6b)$.

TABLE 1

List of the first four natural frequencies

Mode no.	Natural frequencies (Hz)	
	Eqn. (40)	Present
1	17·1	17·1
2	29·7	29·7
3	40·8	40·8
4	57·2	57·1

4.1. MODAL RESULTS

Before proceeding to present any result of this 4-spring problem, first consider a simplified version: only the first spring is attached. This will give an opportunity to check the present formulation in terms of the estimated natural frequencies.

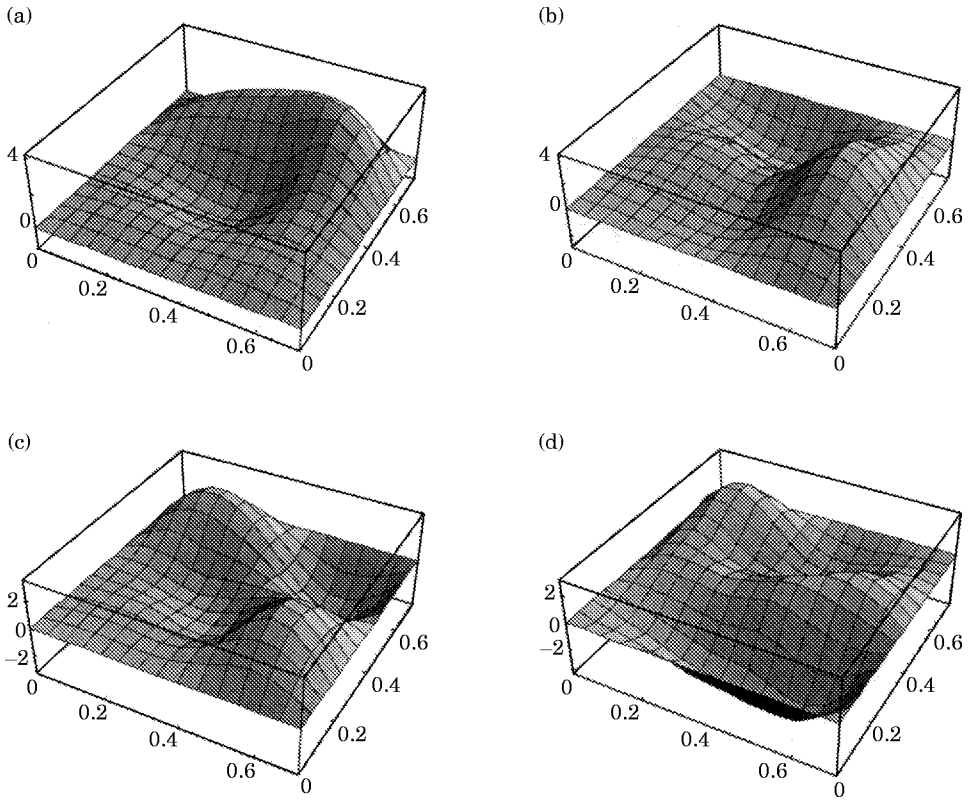

Figure 3. The first four modes of the spring-reinforced plate: (a) mode 1: $f_1 = 46{\cdot}6$ Hz; (b) mode 2: $f_2 = 51{\cdot}0$ Hz; (c) mode 3: $f_3 = 60{\cdot}8$ Hz; (d) mode 4: $f_4 = 71{\cdot}6$ Hz.

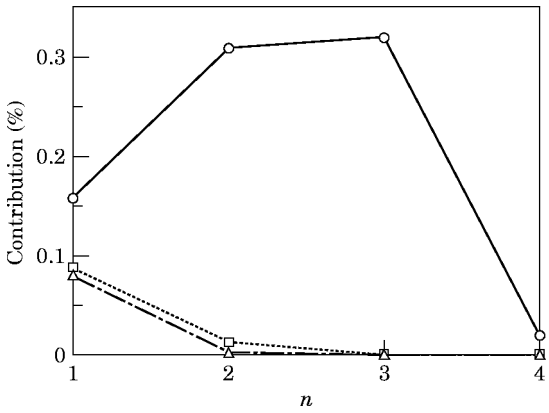

Figure 4. Composition of the first mode: Key: —○—, $m=1$; . . .□ . . . , $m = 2$; —-△-—, $m = 3$.

For this purpose, the characteristic equation given by Das and Navaratna [4] is used here:

$$\frac{-\rho h}{k_1} = \sum_{m,n}^{M,N} \frac{\psi_{mn}^2(x_1, y_1)}{(\omega_{mn}^2 - \omega^2)}. \tag{40}$$

The results obtained from these two different formulations show an excellent agreement as illustrated in Table 1 where the four lowest natural frequencies are listed. A total of 49 modes ($N = M = 7$) is used in both calculations.

Now, return to the original 4-spring case. As stated earlier, the ith mode of the reinforced plate is defined by the function $\boldsymbol{\psi}^{\mathrm{T}}\boldsymbol{\phi}_i$. Since the springs can be viewed as an add-on feature to a simple plate, their effects are basically manifested, from a modal analysis point of view, in altering the original natural frequencies and mode shapes. To see such modifications, the first four modes are plotted in

TABLE 2

The self radiation resistance for the (1,1) *mode calculated by numerical integration and the interpolation approximation*

Wavenumber	Direct	Interpolation	Error (%)
$\Delta k = k_{\max}$			
$k_1 + \Delta k/4$	0·483007	0·482932	0·02
$k_1 + 2\Delta k/4$	0·605405	0·605279	0·02
$k_1 + 3\Delta k/4$	0·727594	0·727479	0·02
$\Delta k = 3k_{\max}$			
$k_1 + \Delta k/4$	0·726594	0·726598	0·00
$k_1 + 2\Delta k/4$	1·05061	1·04864	0·19
$k_1 + 3\Delta k/4$	1·25043	1·24863	0·14
$\Delta k = 5k_{\max}$			
$k_1 + \Delta k/4$	0·953793	0·950223	0·37
$k_1 + 2\Delta k/4$	1·28503	1·27835	0·52
$k_1 + 3\Delta k/4$	1·27400	1·26879	0·41

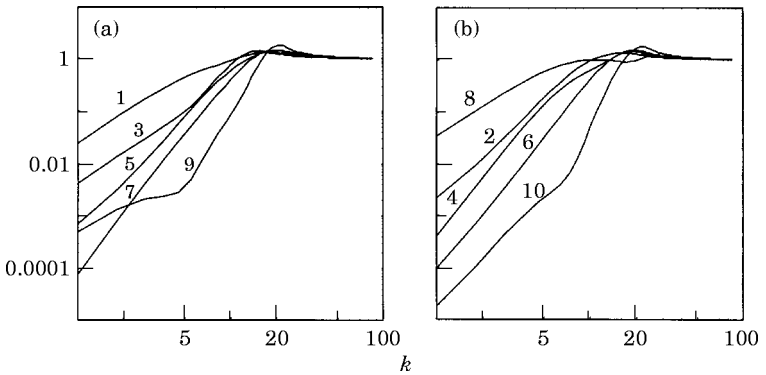

Figure 5. Modal radiation efficiencies for five lowest (a) odd and (b) even modes of the reinforced plate.

Figure 3. Just by looking at these modes, one may be able to identify the traces of some basis modes.

A more vigorous "signature" analysis, however, should rely on the information carried by the vector $\boldsymbol{\phi}_i$ because it completely specifies the position of the ith mode $\boldsymbol{\psi}^{\mathrm{T}}\boldsymbol{\phi}_i$ in the original modal space $\underline{\boldsymbol{\Psi}}$. Because $\|\boldsymbol{\phi}_i\|_2 \equiv 1$, the square of the (m,n)th component of $\boldsymbol{\phi}_i$ can be conveniently used to measure ψ_{mn}'s presentation in the mode $\boldsymbol{\psi}^{\mathrm{T}}\boldsymbol{\phi}_i$. For example, the first mode is replotted in Figure 4 in terms of the contributions of its 12 most dominant basis modes. It can be seen that only a few basis modes actually have a significant influence on it. This is also true for the other modes.

4.2. FREQUENCY INTERPOLATION APPROXIMATION

In order to verify the accuracy of the frequency interpolation approximation discussed in the previous section, Table 2 lists the self-radiation resistance for the (1, 1) mode, calculated at several slave frequencies. The starting master frequency is $f_1 = 150$ Hz ($k_1 a \cong 2$). The ending master frequency is $f_2 = f_1 + \chi k_{\max}$, where χ is an accelerating factor and $k_{\max}(\cong 2)$ is the maximum master frequency step determined from equation (38) with $\epsilon = 0{\cdot}1$ and $N_d = 10$. The slave frequencies are here simply chosen as $k_1 + \chi k_{\max}/4$, $k_1 + \chi k_{\max}/2$ and $k_1 + 3\chi k_{\max}/4$. The results clearly show that the frequency interpolation technique can be used adequately even for a fairly large (master) frequency step.

4.3. MODAL RADIATION EFFICIENCY OF THE REINFORCED PLATE

Once the self and mutual radiation resistances are known for the basis modes, the modal radiation efficiencies for the reinforced plate can be readily determined from equation (23). The radiation efficiencies for the first 10 modes are plotted in Figure 5. In spite of their "irregular" (mode) shapes, they have exhibited a familiar characteristic: reaching to a peak value at some "coincidence" frequency and then consistently descending to unity. Unlike the other modes, the eighth mode shows some peculiarity in that there are two humps on its radiation efficiency curve. The first hump attributes to the (1, 1), (1, 2) and (2, 1) modes which account for an approximate 74% contribution, and the second one occurs

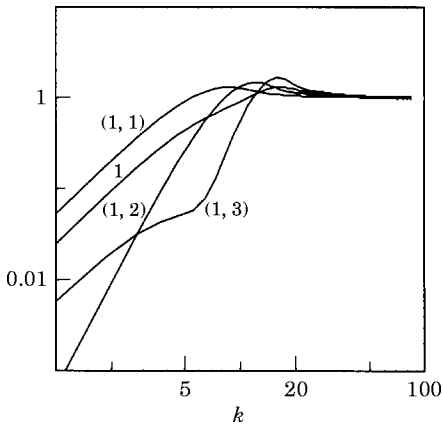

Figure 6. Radiation efficiencies of the first mode and its three most contributory basis modes.

near the coincidence frequencies of the (1, 5) and (5, 1) modes representing another 16% contribution. The dip indicates a lack of contributory basis modes which have coincidence frequencies falling between the two humps.

To understand the occurrence of the humps, the radiation efficiency of the first mode is plotted in Figure 6 together with those of its three most contributory basis modes. Its peak radiation efficiency approximately occurs at the coincidence frequency for the (1, 3) mode. Although the (1, 2) mode has an almost identical presentation in mode 1 as the (1, 3) mode (refer to Figure 4), the resulting radiation efficiency curve does not seem to be very responsive to it, even near its coincidence frequency. Usually, the effectively radiating basis modes are those whose modal wave numbers are not significantly greater than the acoustic wave number for a given frequency. This suggests that only the acoustically fast (basis) modes are likely to be responsible for the hump(s) on a modal radiation efficiency curve. Typically, the higher order modes display a higher and sharper hump at their coincidence frequencies. Since a basis mode will remain to be (radiation) effective after its coincidence frequency, one can infer that the peak radiation efficiency of the mode of the reinforced plate should not occur at a frequency that may exclude

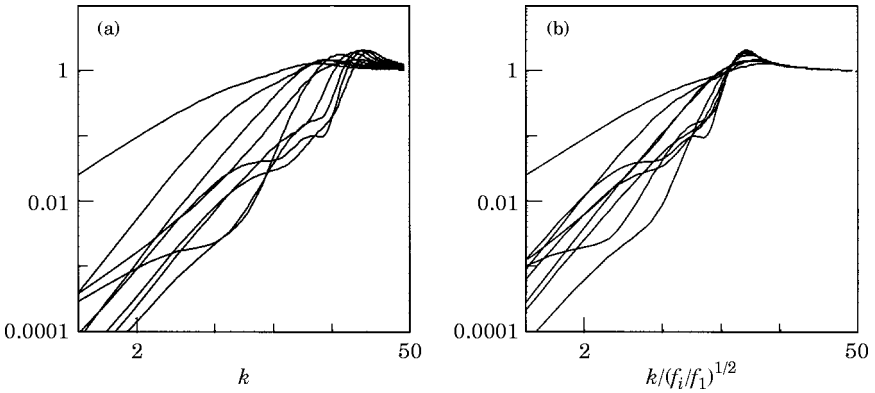

Figure 7. The radiation efficiencies for nine "randomly" selected modes ($i = 1, 4, 7, 10, \cdots, 25$) are plotted by using two different abscissas: (a) k and (b) $k/(f_i/f_1)^{1/2}$.

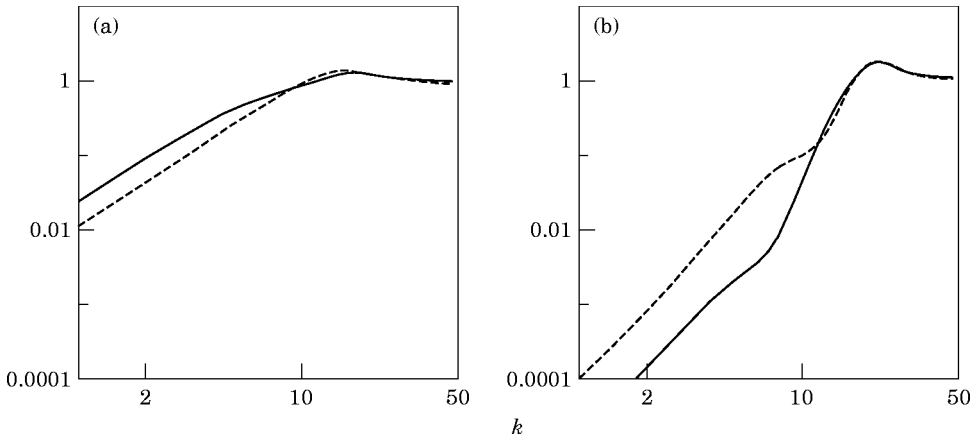

Figure 8. Modal radiation efficiencies for (a) the first and (b) the tenth mode: ——, with cross-modal coupling; - - - -, without cross-modal coupling.

any of the most contributory basis modes from being acoustically fast. Furthermore, by realizing the radiation efficiency of an acoustically fast mode consistently decreases with frequency one can anticipate that the maximum radiation efficiency should occur in the close proximity of the highest of the coincidence frequencies for the contributory basis modes. For example, for a given mode of natural frequency f_i, its contributory basis modes are usually those which satisfy $\omega_{mm} \leqslant 2\pi f_i$. Thus, the frequency $2\pi f_i$ can be used to define a nominal maximum modal wave number for the contributory basis modes, hence the approximate location of the peak radiation efficiency. To verify the point, the radiation efficiencies for the nine "randomly" selected modes ($i = 1, 4, 7, 10, \cdots, 25$) are plotted in Figure 7 by using two different abscissas: k and $k/(f_i/f_1)^{1/2}$. It can be observed that, as the modal order increases, the humps basically shift to the right (high frequency) along the k-axis, and they fall together when the wave number is divided by $(f_i/f_1)^{1/2}$. The pattern for the later case, as shown in Figure 7(b), is frequently presented in the literature when the modal radiation efficiencies of a simple plate are plotted as functions of the wave number ratios (the acoustic wave numbers divided by the modal wave numbers). In this way, the "coincidence" frequencies become predictable for the modes of the loaded plate.

4.4. EFFECTS OF THE CROSS-MODAL COUPLING

In order to understand the effects of the cross-modal coupling among the basis modes, the radiation efficiencies for the first and tenth modes of the loaded plate are plotted in Figure 8, which are calculated, respectively, with and without including the mutual radiation resistances. The results clearly indicate that, except for high frequencies, the effects of the cross-modal coupling is normally meaningful. Furthermore, it should be noted that the contributions of the mutual radiation resistances can be either positive or negative, which implies, without accounting for the cross-modal contributions, that the modal radiation efficiencies of the loaded plate can be over- or under-estimated at a given frequency.

The acoustic power radiated from the loaded plate can be determined in the same way as the modal radiation efficiency. However, it should be mentioned that, unless for other uses, the modal radiation efficiencies need not to be explicitly calculated for the determination of sound power. As a matter of fact, it will be more efficient in the present case to directly calculate the sound power from the coefficient vector **A** and the radiation resistance matrix $\Re[Z]$.

5. SUMMARY

The vibration of a simply supported rectangular plate reinforced by a finite number of springs at arbitrary points can be conveniently expressed as a linear combination of the basis modes for the corresponding simple plate. Both the natural frequencies and mode shapes for the spring-reinforced plate can be simultaneously obtained by solving a standard eigen-problem. A linear relationship exists between the two modal groups, which allows to study the radiation characteristic of a loaded plate in terms of that of a simple plate. Thus, the most time-consuming calculation (of the radiation resistances matrix) needs to be carried out only once when a plate is subjected to various reinforcing plans and/or a multiple of loading conditions.

It has been shown that the frequency interpolation technique works well for (even) fairly large master frequency steps. Consequently, the intensive numerical integrations are now limited only to a small number of master frequencies. Like in a simple plate case, the modal radiation efficiency curve typically display a hump near the "coincidence" frequency determined by a maximum nominal wave number for the contributory basis modes, and then asymptotically descends to unity. The effects of the cross-modal coupling between the basis modes normally need to be considered in studying the acoustic characteristic of a loaded plate. Although the current discussions have been focused on the spring-loaded plates, it should be straightforward to extend them to plates with some other features such as a combination of masses and springs.

REFERENCES

1. H. Cohen and F. Handelman 1956 *Journal of Franklin Institute* **261**, 319–329. Vibrations of a rectangular plate with distributed added mass.
2. C. L. Amba-Rao 1964 *Journal of Applied Mechanics* **31**, 550–551. On the vibration of a rectangular plate carrying a concentrated mass.
3. Y. C. Das and D. R. Navaratna 1963 *Journal of Applied Mechanics* **30**, 31–36. Vibrations of a rectangular plate with concentrated mass, spring, and dashpot.
4. W. F. Stokey and C. F. Zorowski 1959 *Journal of Applied Mechanics* **26**, 210–216. Normal vibrations of a uniform plate carrying any number of finite masses.
5. J. S. Wu and S. S. Luo 1997 *Journal of Sound and Vibration* **200**, 179–194. Use of the analytical-and-numerical-combined method in the free vibration analysis of a rectangular plate with any number of point masses and translational springs.
6. W. L. Li and H. J. Gibeling 1997 *Proceedings of* 15*th International Modal Analysis Conference* **2**, 1966–1972. Vibro–acoustic analysis of a rectangular plate elastically reinforced at arbitrary points.
7. A. Leissa 1993 *Vibration of Plates*. Acoustical Society of America.

8. C. E. Wallace 1972 *Journal of the Acoustical Society of America* **51**, 946–952. Radiation resistance of a rectangular panel.
9. M. C. Gomperts 1974 *Acustica* **30**, 320–327. Radiation from rigid baffled rectangular plates with general boundary conditions.
10. A. Berry, J. Guyader and J. Nicolas 1990 *Journal of the Acoustical Society of America* **88**, 2792–2802. A general formulation for the sound radiation from rectangular, baffled plates with arbitrary boundary conditions.
11. T. Takahagi, M. Nakai and Y. Tamai 1995 *Journal of Sound and Vibration* **185**, 455–471. Near field sound radiation from simply supported rectangular plates.
12. H. Levine 1984 *Journal of the Acoustical Society of America* **76**, 608–615. On the short wave acoustic radiation from planar panels or beams of rectangular shape.
13. R. F. Keltie and H. Peng 1987 *Journal of Vibration Acoustics and Stress Reliability in Design* **109**, 48–54. The effects of modal coupling on the acoustic power radiation from panels.
14. S. Snyder and N. Tanaka 1984 *Journal of the Acoustical Society of America* **97**, 1702–1709. Calculating total acoustic power output using modal radiation efficiencies.
15. W. L. Li and H. J. Gibeling submitted to *Journal of the Acoustical Society of America*. Determination of the effects of cross-modal coupling on the acoustic power radiation from a rectangular plate.
16. G. W. Benthien and H. A. Schenck 1991 *Boundary Elements Methods in Acoustics*, chapter 6. London: Elsevier Applied Science; Computational Mechanics Publications, Southampton.